UC Santa Cruz
UC Santa Cruz Previously Published Works

Title

Protein Sequence and Membrane Lipid Roles in the Activation Kinetics of Bovine and Human Rhodopsins

Permalink

Journal

ISSN

Authors

Szundi, Istvan
Funatogawa, Chie
Guo, Ying
et al.

Publication Date

DOI

Protein Sequence and Membrane Lipid Roles in the Activation Kinetics of Bovine and Human Rhodopsins

Istvan Szundi,[1] Chie Funatogawa,[1] Ying Guo,[2] Elsa C. Y. Yan,[2] and David S. Kliger[1,*]

[1]Department of Chemistry and Biochemistry, University of California, Santa Cruz, Santa Cruz, California and [2]Department of Chemistry, Yale University, New Haven, Connecticut

ABSTRACT   Rhodopsin is a G protein-coupled receptor found in the rod outer segments in the retina, which triggers a visual response under dim light conditions. Recently, a study of the late, microsecond-to-millisecond kinetics of photointermediates of the human and bovine rhodopsins in their native membranes revealed a complex, double-square mechanism of rhodopsin activation. In this kinetic scheme, the human rhodopsin exhibited more Schiff base deprotonation than bovine rhodopsin, which could arise from the ~7% sequence difference between the two proteins, or from the difference between their membrane lipid environments. To differentiate between the effects of membrane and protein structure on the kinetics, the human and bovine rhodopsins were inserted into 1-palmitoyl-2-oleoyl-*sn*-glycero-3-phosphocholine lipid nanodiscs and the kinetics of activation at 15°C and pH 8.7 was investigated by time-resolved absorption spectroscopy and global kinetic analysis. For both proteins, the kinetics in nanodiscs shows the characteristics observed in the native membranes, and is described by a multisquare model with Schiff base deprotonation at the lumirhodopsin I intermediate stage. The results indicate that the protein sequence controls the extent of Schiff base deprotonation and accumulation of intermediates, and thus plays the main role in the different activation kinetics observed between human and bovine rhodopsins. The membrane lipid does have a minor role by modulating the timing of the kinetics, with the nanodisc environment leading to an earlier Schiff base deprotonation.

INTRODUCTION

The visual pigment rhodopsin is a membrane-bound protein responsible for initiating the process of dim-light vision in the rod cells of the retina. It is a light-activated G protein-coupled receptor containing an 11-*cis* retinal chromophore covalently bound through a protonated Schiff base linkage to lysine 296. Upon light absorption, this chromophore is photoisomerized to form an all-*trans* protonated retinal Schiff base, initiating a series of protein changes leading to conversion of the protein to its active form. The active form then binds to transducin, initiating an enzyme cascade resulting in a greatly amplified visual signal (1). The photoactivation of rhodopsin after the photoisomerization of the chromophore has been studied extensively throughout the years. Early studies, using low-temperature trapping methods, suggested a simple linear activation mechanism (Fig. S1) (2,3).

In recent years, the activation mechanism of rhodopsin has been studied under more physiologically relevant temperature conditions. This has resulted in the simple mechanism being expanded to a more complex, branched square model, and recently, to a double-square scheme (Fig. 1) (4–8). In this kinetic model, the photoisomerization of rhodopsin is followed by formation of a red-shifted intermediate, bathorhodopsin, emerging on the subpicosecond timescale (9–11). The bathorhodopsin intermediate enters into an equilibrium with a blue-shifted intermediate, resulting from relaxation of a twisted to a planar chromophore at ~50 ns (12,13). This is followed by the equilibrium between two lumirhodopsin (Lumi) intermediates, Lumi-I and Lumi-II, which forms in the nanoseconds to early microseconds timescale (6). The equilibrium mixture then branches to form the intermediates shown in Fig. 1, which include 480-nm absorbing metarhodopsin I (Meta-Ia$_{480}$) and a 380-nm absorbing metarhodopsin I-like intermediate with a deprotonated Schiff base (Meta-I$_{380}$) (5). These intermediates subsequently convert into a second metarhodopsin I (Meta-Ib$_{480}$) and two metarhodopsin II intermediates (Meta-IIa and Meta-IIb) (5), best observed at moderately alkaline pH and low temperature.

CrossMark

Rho $\longrightarrow$ Batho $\rightleftarrows$ BSI

Lumi I $\rightleftarrows$ Lumi II $\rightleftarrows$ Meta I$_{380}$

Meta Ia$_{480}$ $\rightleftarrows$ Meta IIa

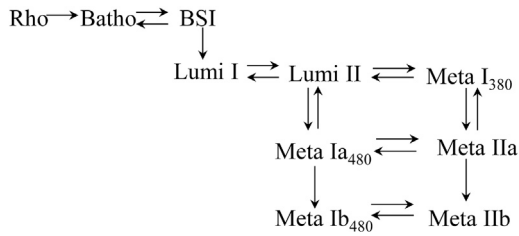Meta Ib$_{480}$ $\rightleftarrows$ Meta IIb

FIGURE 1 The double-square scheme for the photoactivation of rhodopsin.

The isospectral intermediates, Meta-Ia$_{480}$/Meta-Ib$_{480}$ and Meta-IIa/Meta-IIb, could be a result of further chromophore relaxations, movement of the transmembrane helices, and/or the rearrangement of the hydrogen-bonding network (14–20). Studies also show that the movement of transmembrane helix-6 could be the crucial step leading to the active form of the protein (21,22). In the double-square model it could possibly occur in one of the transitions connecting the last four intermediates, Meta-Ia$_{480}$, Meta-Ib$_{480}$, Meta-IIa, and Meta-IIb.

Historically, many studies have been carried out on bovine rhodopsin because of its availability and its high sequence homology ($\sim$93%) to the human protein (23,24). The photoactivation mechanisms of bovine and human rhodopsins were shown to follow the same kinetic model (Fig. 1) at 15°C, although they exhibit differences in their actual reaction rates (5,25). Human rhodopsin activation favors a path involving more of the deprotonated Schiff base intermediates than the bovine protein. Specifically, the equilibrium at the early Schiff base deprotonation steps are forward shifted in comparison to the bovine rhodopsin (25,26).

Differences in the kinetics observed between human and bovine rhodopsins lead to the question of to what extent these differences are related to protein sequence variations and to the dissimilarities of the lipid membranes in which these two proteins are embedded. Despite the 93% sequence homology of the bovine and human rhodopsins, there are minor sequence differences that can be important in shaping the kinetics (25,26).

Both human and bovine rod outer segment (ROS) membranes are comprised of different ratios of phosphatidylcholine (PC), phosphatidylethanolamine (PE), phosphatidylserine, and phosphatidylinositol (27–29). The membrane compositions of human and bovine ROS are similar, but not identical (30). Furthermore, age and diet also effect the lipid composition (31). The lipid-rhodopsin interactions and the effect of varying lipids have been shown to result in significant changes in the equilibrium between the intermediates in the activation mechanism, especially the equilibrium of the Schiff base deprotonation at the final metarhodopsin I to metarhodopsin II stage (28,29). Bovine and human membrane samples also have different histories. Human rhodopsin has generally been exposed much longer to light and oxygen during preparation

than bovine rhodopsin samples. Under these conditions some degradation of polyunsaturated lipids is possible, and the extra retinal added to reconstitute human rhodopsin may affect the membrane integrity and composition in a way that results in enhanced deprotonation of the Schiff base in human rhodopsin, and thus contributes to the differences in kinetics observed in native membranes.

The question of which of the kinetic differences between bovine and human rhodopsins in their native membranes are caused by the $\sim$7% sequence difference between the two proteins, and which ones are related to the lipids in the membranes, is an important one for understanding the protein structure-function relationship. To answer this question, we investigated the activation kinetics of both proteins in nanodiscs (32), also known as discoidal reconstituted high-density lipoprotein (33) and nanoscale apolipoprotein-bound bilayer (34). In the nanodiscs the original membrane lipids were diluted by an over tenfold excess of 1-palmitoyl-2-oleoyl-sn-glycero-3-phosphocholine (POPC), thus making the lipid environments of bovine and human rhodopsins practically the same. The results suggest that protein sequence and structure play a major role in shaping the activation kinetics. Because small changes in the function of rhodopsin resulting from sequence differences can lead to retinal diseases, such as retinitis pigmentosa (35,36), it is crucial to understanding the effect of various components on the activation of rhodopsin.

MATERIALS AND METHODS

The native bovine and human rhodopsins were prepared as previously described in detail (7,37,38). After the extrinsic membrane proteins were removed by washing the ROS two to three times with 1 mM EDTA (pH 7), the ultraviolet-visible absorption spectra are measured. $\sim$1.5 mg of washed ROS was pelleted by centrifugation (17,000 $\times$ g for 25 min) and the buffer was exchanged by resuspending the pellet in a final solution of 50 mM sodium phosphate (pH 6.5) in 0.5% n-dodecyl-β-D-maltoside (from Anatrace).

Preparation of membrane scaffold protein

To prepare membrane scaffold protein (MSP) for assembling nanodiscs, the plasmid inserted with the MSP1E3D1 (39) gene tagged with the TEV cleavage site and 6$\times$ His purification tag was transformed into the BL21-Gold cells (Stratagene) (40,41). The cells were incubated at 37°C. Once the absorbance at 600 nm reached $\sim$0.8, isopropyl β-D-1-thiogalactopyranoside was added to media to induce protein expression. After a 4-h induction period, cells were harvested and sonicated. The lysate was centrifuged. The supernatant was loaded onto an Ni-NTA column. After washing, the protein was eluted followed by removal of the His6 tag by the TEV protease (42). MSP was stored at 4°C for future nanodisc preparation.

Nanodisc assembly

A DC protein assay kit (Bio-Rad, Hercules, CA) was used to determine the total protein concentration from the resuspended solution containing rhodopsin. Based on the total protein concentration, nanodisc assembly mixture was prepared as 90 μM MSP, 8 mM POPC (Avanti Polar Lipids,

Alabaster, AL) solubilized in 180 mM n-dodecyl-β-D-maltoside, and ~0.44 μg/μL total protein in buffer containing 50 mM Tris (pH 7.4), 135 mM NaCl, 5 mM CaCl$_2$, 5 mM MgCl$_2$, 4 mM EDTA, and 4% glycerol. After incubation of the mixture on ice for 30 min, ~10-fold excess (by mass) of Bio-Beads SM-2 resin (Bio-Rad) were added to efficiently remove detergents for nanodisc formation (43). After overnight incubation with Bio-Beads, bench-top centrifuge was used to separate the nanodisc mixture from Bio-Beads. The transmission electron microscopy (TEM) images of the nanodiscs after the incorporation of rhodopsin are shown in Fig. S2 *a*. The size exclusion chromatogram of nanodiscs containing rhodopsin shows a major peak corresponding to a Stokes diameter of ~12 nm (Fig. S2 *b*). The ratio of rhodopsin-filled nanodiscs to empty nanodiscs is estimated to be roughly 1:4, assuming single-protein occupancy. Because the "empty" nanodiscs were not photoreactive, they did not contribute to the spectral changes and thus were not removed. To minimize the potential influence of native membrane lipids (Mlipid) on the kinetics, there is a high ratio of POPC lipids to the native lipids. Based on the disc size and the dimensions of rhodopsin and lipid molecules, the ratio of rhodopsin/MSP/Mlipid/POPC is estimated to be 1:2:16:180 for the discs containing rhodopsin. The buffer of the nanodiscs samples was exchanged, using an Amicon ultra 0.5 mL centrifugal filter (Sigma-Aldrich, St. Louis, MO), and stored in a buffer containing 10 mM Bis-Tris propane and 100 mM NaCl (pH 7). The pH of the sample was adjusted to 8.7 at 15°C before the time-resolved optical absorption (TROA) measurements.

TROA measurements and analysis

The TROA difference spectra (postphotolysis $-$ prephotolysis) were measured between 300 and 700 nm using the apparatus described previously (7,12). The sample temperature was maintained at 15°C during the TROA measurements with a water bath. The difference spectra were recorded between delay times of 10 μs to 120 ms after photoexcitation from a 477-nm dye laser (~1 mJ per pulse, 7 ns) pumped with the third harmonic of a Nd:YAG laser. The probe light was polarized at 54.7° (magic angle) to prevent absorbance changes due to the rotational diffusion of rhodopsin (44).

The data matrix representing the TROA data at all delay times was subjected to singular value decomposition followed by global exponential fitting and kinetic modeling, as described previously and outlined in the Supporting Material (5,12,25,45). All calculations were performed using programs written in MATLAB (The MathWorks).

RESULTS

TROA difference spectra were collected at 15°C (pH 8.7) for both bovine and human rhodopsins embedded in nanodiscs, and are displayed from 330 to 660 nm in Fig. 2, *a* and *b*, respectively. These conditions were chosen because they have been shown to reveal the full array of rhodopsin intermediates upon photolysis. The spectra were recorded at 12 delay times of 10, 25, 50, 100, and 500 μs, and 1, 2, 5, 10, 20, 50, and 120 ms after laser excitation. The directions of absorption change over time in different spectral regions are indicated by the arrows.

Global exponential fitting of experimental data

The experimental data for both proteins were best fit with four exponentials having lifetimes of 19 μs, 420 μs, 3.1 ms, and 120 ms for the bovine, and 22 μs, 310 μs,
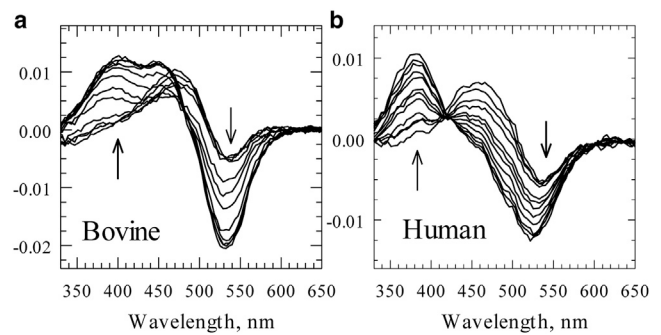

FIGURE 2 Time-resolved (postphotolysis $-$ prephotolysis) difference spectra of (*a*) bovine and (*b*) human rhodopsins in nanodiscs at 15°C and pH 8.7. The difference spectra were recorded at 12 delay times of 10, 25, 50, 100, and 500 μs and 1, 2, 5, 10, 20, 50, and 120 ms after laser excitation. The arrows indicate the direction of spectral change as time progresses.

6.1 ms, and 120 ms for human rhodopsin embedded in nanodiscs. Because of sample limitations, the uncertainties in the values of the longest, 120-ms lifetimes can be as high as a factor of 2. The late spectral changes associated with these lifetimes, however, were clearly present in the experimental data. For the same reason, the first lifetimes are uncertain within a factor of 1.5, and the other lifetimes within a factor of 1.2. The amplitude spectra, also called *b*-spectra, associated with the lifetimes are shown in Fig. 3, *a* and *b* for the bovine and human rhodopsin samples, respectively. The final *b*-spectra, b_0, represent the spectra of the end products for the proteins in our experimental time range. The residual
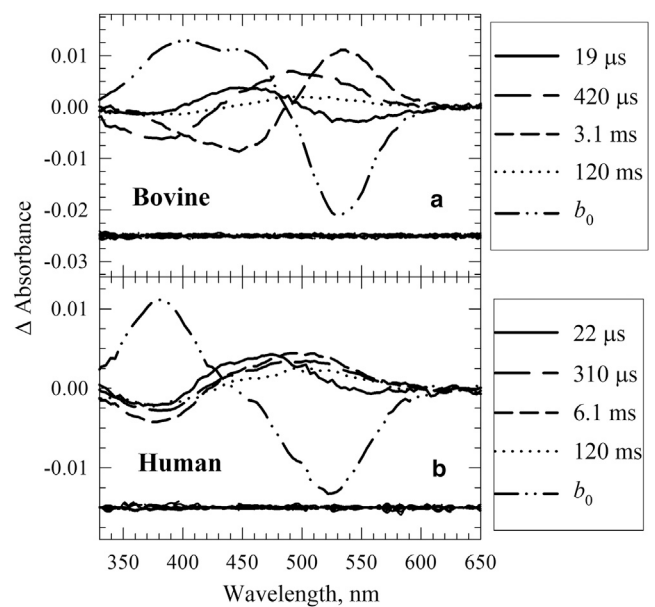

FIGURE 3 *b*-spectra and apparent lifetimes determined from the global exponential fit for (*a*) bovine and (*b*) human rhodopsins in nanodiscs. The line type of the lifetime listed next to each panel corresponds to the *b*-spectrum line type. b_1 (19 or 22 μs), b_2 (420 or 310 μs), b_3 (3.1 or 6.1 ms), b_4 (120 ms), and b_0. b_0 represents the spectrum of the end product for the experimental timescale. The residuals of the four exponential fit are shown below the *b*-spectra in each panel.

FIGURE 5 A comparison of the first *b*-spectrum of the (*a*) bovine and (*b*) human rhodopsins in nanodiscs (*solid lines*), and in the native membrane (*broken lines*). (*c*) The difference between the first *b*-spectrum of the human rhodopsin in nanodiscs and membrane (*dotted lines*) is compared with the normalized second *b*-spectrum of human rhodopsin in nanodiscs (*broken lines*).

Description of kinetics by the eight-membered multisquare scheme

The kinetics of both bovine and human rhodopsins in their native membrane environments have been described by the double-square model (Fig. 1), which was created by adding a second Meta-I$_{480}$ and a second deprotonated metarhodopsin II intermediate to the original square model (5,25). The need for the new intermediates in the kinetic scheme was based on the analysis of *b*-spectra. Generally, positive spectral contributions to the *b*-spectra reflect the decay and negative ones reflect the formation of intermediates (45). The shapes of the late-millisecond *b*-spectra revealed the formation of a second Meta-I$_{480}$ intermediate, and thus provided the crucial information leading to the new model. To test whether bovine and human rhodopsins in nanodiscs follow the same complex kinetics, we compared the longest, 120-ms *b*-spectra in nanodiscs to the corresponding late-millisecond *b*-spectra reported for the native membrane samples (Fig. 4, *a* and *b*, *solid and broken lines*, for bovine and human rhodopsin, respectively). For both rhodopsins, the *b*-spectrum in the nanodiscs has the same shape as the normalized *b*-spectrum in the native membrane, which indicates two Meta-I$_{480}$ intermediates in the kinetics, as described by the double-square model.

The first intermediate in the double-square model, Lumi-I, decays into Lumi-II in a reversible step. The first *b*-spectra for the bovine rhodopsin in nanodiscs and in native membrane (Fig. 5 *a*, *solid and broken lines*, respectively) are practically the same: both show a Lumi-I − Lumi-II difference spectrum expected for the first step in the scheme. This is not the case for the human rhodopsin in nanodiscs. As seen in Fig. 5 *b*, the first *b*-spectrum (*solid line*) has a shape more complex than the one observed in the native membrane (*broken line*). The difference between these two *b*-spectra (Fig. 5 *c*, *dotted line*) is very similar
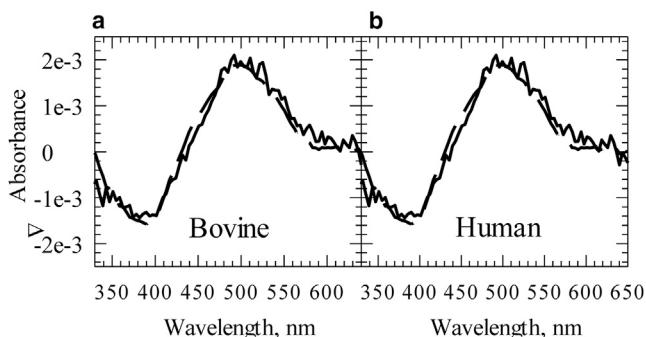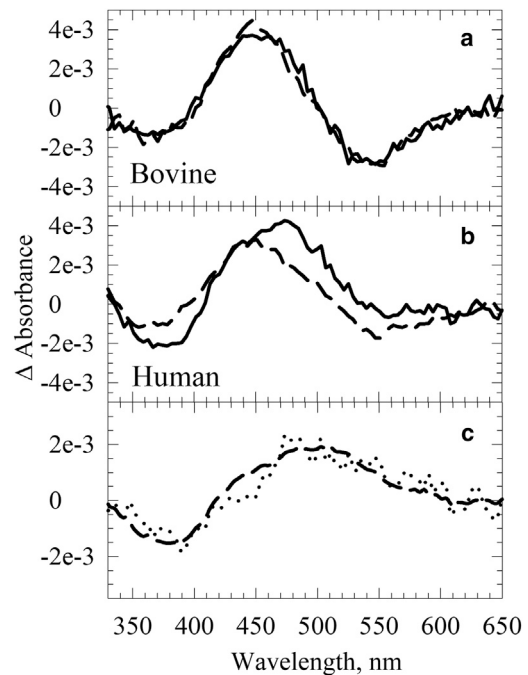

FIGURE 4 A comparison of the 120-ms *b*-spectrum of the (*a*) bovine and (*b*) human rhodopsins in nanodiscs (*solid lines*) with the corresponding *b*-spectrum in the native membrane (*broken lines*), normalized to the same amplitude.

in shape to the second *b*-spectrum for human rhodopsin in nanodiscs (Fig. 5 *c*, *broken line*). Based on its shape and lifetime, the latter *b*-spectrum can be assigned to the formation of the Meta-I$_{380}$ intermediate from the Lumi-I/Lumi-II mixture. Thus, the first *b*-spectrum for the human rhodopsin in nanodiscs shows the formation of Lumi-II, and simultaneously, the formation of a deprotonated, 380-nm absorbing intermediate from Lumi-I. The superposition of two transitions in one *b*-spectrum is typical of branching (45), this time at the Lumi-I state. The new 380-nm absorbing intermediate, to which Lumi-I is branching, we name Lumi$_{380}$. By adding this new intermediate to the double-square model, it becomes an eight-membered multisquare model (Fig. 6). We assume that this model is valid not only for the human but also for the bovine rhodopsin in nanodiscs, even though the accumulation of the Lumi$_{380}$ intermediate remains below detection limits.

Using model spectra for the intermediates, the microscopic rate constants in the eight-membered multisquare scheme for the bovine and human rhodopsins in nanodiscs were obtained by a fitting process which reproduced both the experimental *b*-spectra and lifetimes (5). As discussed in our earlier report (5), the fit does not give a unique solution to the kinetics because the number of experimental *b*-spectra and lifetimes are less than required by the eight-membered model (see Supporting Material). Multiple

Lumi I ⟶ Lumi$_{380}$

Lumi II ⟶ Meta I$_{380}$

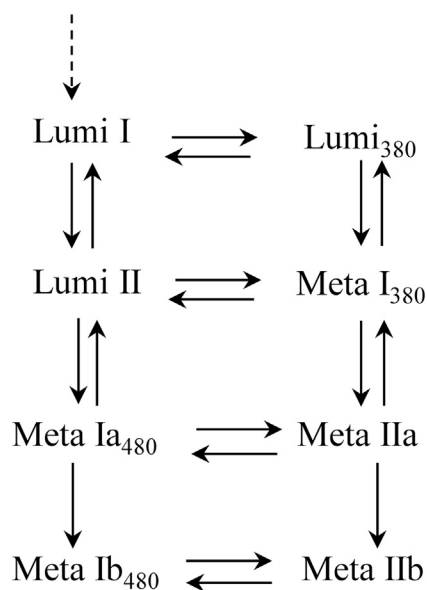Meta Ia$_{480}$ ⟶ Meta IIa

Meta Ib$_{480}$ ⟶ Meta IIb

FIGURE 6 The eight-membered multisquare scheme for the late intermediates for the photoactivation of rhodopsin in nanodiscs.

solutions, or submodels, arise from spectral and temporal degeneracies due to the presence of isospectral intermediates in the scheme (5). Here, we present only the case of degenerate lifetimes, which has a straightforward physical interpretation. In this case, some of the spectral transitions present in the kinetics can occur with very similar lifetimes and cannot be separated in the exponential fitting, thus resulting in a reduced number of exponentials. This kinetic pattern was also evaluated in our previous work (25), and will be used as basis for comparison between the rate constants of a few individual reaction steps obtained for the two rhodopsins in native membranes and nanodiscs.

Out of the four experimental lifetimes, the first one is taken to be degenerate because branching of Lumi-I into Lumi-II and the new Lumi$_{380}$ intermediate is observed in the first b-spectrum for the human rhodopsin. The third and fourth lifetimes are also taken to be degenerate because the two Meta-I$_{480}$ intermediates evolve in the millisecond time range. The second experimental lifetime and b-spectrum is not considered degenerate and is assigned to a single process, the Meta-I$_{380}$ formation from the Lumi-I/Lumi-II mixture. The b-spectrum corresponding to this reaction step is not observed in the native membrane at 15°C because the accumulation of the Meta-I$_{380}$ intermediate there remains below detection limits (5,8,25). The reproduced b-spectra pairs that correspond to a degenerate lifetime are summed up before the reproduced and the experimental b-spectra are compared. Fig. S3, a and b show the quality of the fit for the set of microscopic rate constants displayed in Table S1 for the bovine and human rhodopsin in nanodiscs, respectively. A simplified multisquare scheme, in which Lumi-I converts to Meta-I$_{380}$ directly, is also feasible mathematically, but because of the problems associated with

its physical interpretation, it is not presented here (see details in Supporting Material).

DISCUSSION

In a recent kinetic study on bovine rhodopsin in its native membrane (5), we found that at alkaline pH (pH 8.7) and moderately low temperature (15°C), new intermediates and reaction steps, which remained masked at neutral pH and higher temperatures, became visible. The experimental data revealed the presence of two metarhodopsin I intermediates, named Meta-Ia and Meta-Ib, Meta-Ia being in equilibrium with a Lumi-II intermediate. To accommodate the new intermediates and reaction steps, the original square kinetic model was extended into a double-square model (Fig. 1). Application of this model to the experimental data showed that multiple solutions, named submodels, were possible because of the presence of isospectral intermediates in the reaction scheme. Although the submodels contained different sets of microscopic reaction rate constants, they all produced the same time dependence of the intermediate concentrations, and thus they all reproduced the exponential time dependence of the experimental data, including the apparent rates (or lifetimes) and the amplitude spectra (b-spectra).

In a subsequent study (25), we compared the kinetics of bovine and human rhodopsins in their native membrane environments. We found that human rhodopsin also followed the complex kinetics represented by the double-square model. However, it showed elevated levels of Schiff base deprotonation along the reaction pathway and also a higher degree of reversibility in the transition between Lumi-II and Meta-Ia intermediates. As in case of bovine rhodopsin, multiple solutions, each having its own set of microscopic reaction rate constants, were consistent with the experimental data.

In this study, bovine and human rhodopsins were inserted into nanodiscs with practically the same lipid composition and their kinetics were investigated at 15°C (pH 8.7), which was found earlier to reveal the most kinetic details. We found that both proteins follow the kinetics described by an eight-membered multisquare model (Fig. 6), an extension of the double-square model mentioned above. As in the case of the native membrane, there are kinetic differences between the two proteins, including the extent of deprotonation of the Schiff base along the reaction pathway and the degree of reversibility of the Lumi-II-to-Meta-Ia step.

A comparison of the kinetics for bovine and human rhodopsins in both native membrane and nanodiscs, composed predominantly by the same PC lipid, allows us to distinguish between the kinetic effects caused by membrane lipids and the ones induced by the proteins themselves. As already mentioned, the kinetic fit does not produce a unique solution for either of the proteins and

thus there are multiple kinetic solutions consistent with the experimental data. Because each of the solutions has a different set of microscopic rate constants, a direct and quantitative comparison between bovine and human rhodopsins, or between the different lipid environments, is not feasible at the level of microscopic rate constants of the individual steps in the kinetic scheme. Therefore, we analyzed and compared the b-spectra and the apparent rates, which are reproduced by all submodels, in terms of the kinetic steps contained in the eight-membered multisquare model (Fig. 6). We cite microscopic reaction rate constants only to estimate differences in equilibria for the two proteins. To better visualize the differences in the kinetics for the two proteins we also inspected and compared the time-dependent concentrations of the intermediates, and refer to the time dependence of the total reaction flow through the individual steps involved in the buildup and decay of concentrations of the intermediates in the kinetic schemes.

Connection between spectral changes in b-spectra and physical steps in the reaction chain in nanodiscs and native membranes

Bovine rhodopsin

The b-spectra for bovine rhodopsin in nanodiscs and native membrane are shown in Fig. 7 a, with solid and dotted lines, respectively. The fastest apparent process deduced from the first b-spectra (b_1 lines) represents the decay of Lumi-I into Lumi-II. It has similar lifetimes, 19 and 23 μs in nanodiscs and in native membrane, respectively. The two spectra are of the same size, which reflects very similar level of net con-
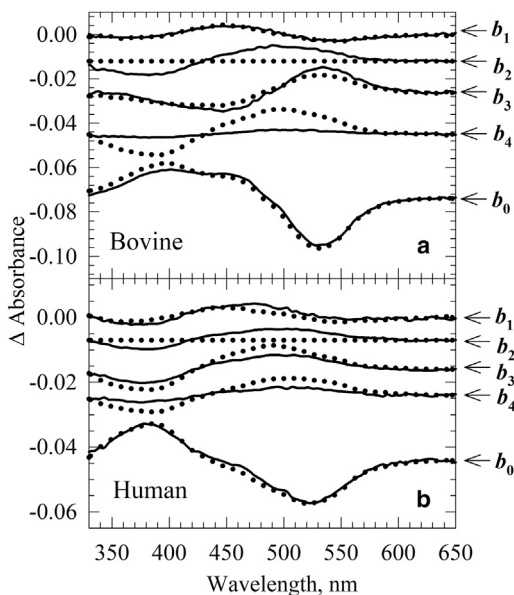
version from Lumi-I into Lumi-II in the two membranes, leading to similar equilibria between these two intermediates. Thus, this early process was not significantly influenced by the replacement of the native membrane lipids with artificial ones. As a consequence, the time evolution of the Lumi-I and Lumi-II intermediates shown in Fig. 8 a (*blue and red curves*, respectively) are practically the same in the nanodiscs and native membrane environments (*solid and dotted lines*, respectively). For easier comparison, the first lifetime in native membrane was set to the nanodiscs value of 19 μs. For the native membrane the deprotonated Lumi intermediate, Lumi$_{380}$ in Fig. 6, was not observed. Although the first b-spectrum for the bovine nanodiscs did not suggest the presence of this intermediate explicitly, we included it in the model because it was clearly observed for the human nanodiscs sample. The flow from Lumi-I to Lumi$_{380}$ shows that branching of Lumi-I toward Lumi$_{380}$ for bovine rhodopsin in nanodiscs is small, as expected, but still noticeable (Fig. 9; Fig. S4 c, *blue solid line*). It is, however, not sufficient to build up detectable concentration for the latter intermediate (Fig. 8 a, *brown solid line*, obscured by the time axis) because of its fast conversion into Meta-I$_{380}$.

The second b-spectrum, with 420 μs apparent lifetime, observed in nanodiscs was absent in the native membrane (Fig. 7 a, b_2 *solid and dotted curves*, respectively). It reflects the transition of Lumi-I/Lumi-II mixture to Meta-I$_{380}$, which in native membrane becomes insignificant at low temperature. There, we introduced a b-spectrum having

FIGURE 7 The b-spectra for (*a*) bovine and (*b*) human rhodopsins in nanodiscs (*solid lines*) and the native membrane (*dotted lines*).
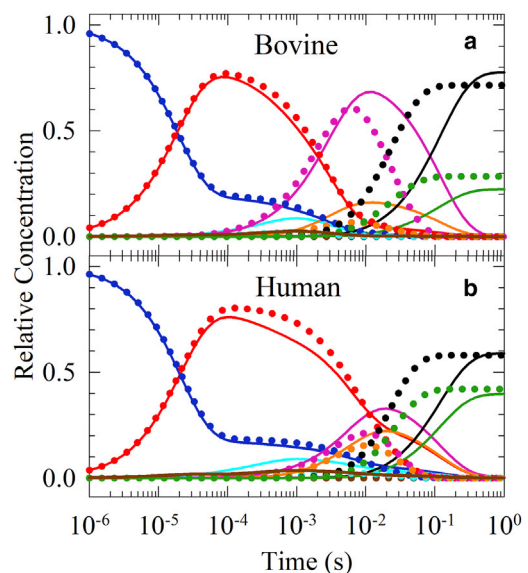

FIGURE 8 A comparison of the time evolution of intermediates in the multisquare kinetic model for nanodiscs (*solid lines*) and in the double-square model for native membrane (*dotted lines*) for (*a*) bovine and (*b*) human rhodopsins. The concentration profiles of Lumi-I (*blue*), Lumi$_{380}$ (*brown*), Lumi-II (*red*), Meta-I$_{380}$ (*cyan*), Meta-Ia$_{480}$ (*magenta*), Meta-IIa (*orange*), Meta-Ib$_{480}$ (*black*), and Meta-IIb (*green*) spectral forms are displayed between 1 μs and 1 s. To see this figure in color, go online.
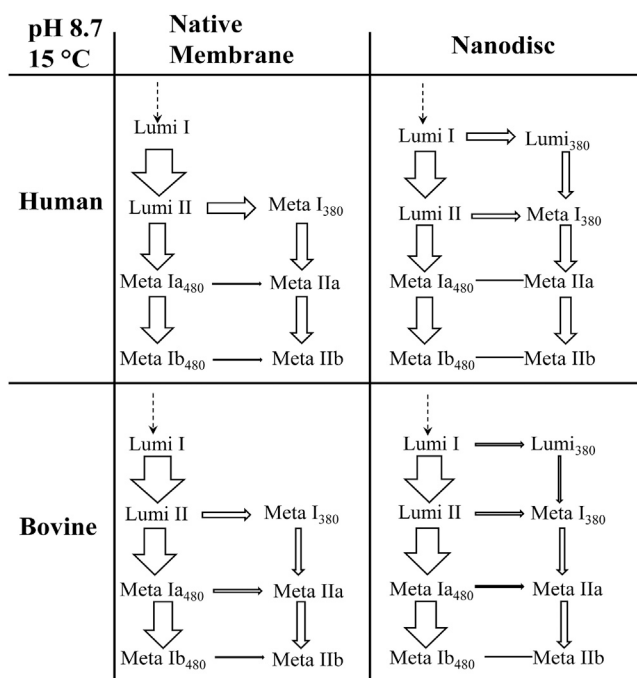
FIGURE 9 Comparison of the net flow through the later-microsecond to millisecond timescale transitions for bovine and human rhodopsins at pH 8.7 and 15°C in the native membrane and nanodiscs is visualized using arrows. The thickness of the arrows correlates with the amount of flow through those intermediates.

negligible amplitude and 250 μs lifetime, to allow reaction flow through the Meta-I$_{380}$ intermediate in the double-square model (5). In nanodiscs this b-spectrum has a significant amplitude and consequently, the concentration of Meta-I$_{380}$ (Fig. 8 a, $cyan$ $solid$ $line$) becomes significant. The flow through the Lumi-I-to-Lumi$_{380}$ step, and the faster Lumi$_{380}$-to-Meta-I$_{380}$ step that follows it, is comparable to the flow through the Lumi-II-to-Meta-I$_{380}$ step (Fig. 9; Fig. S4 c, $blue$ and $green$ $solid$ $lines$, respectively).

The third b-spectra, with lifetimes of 3.1 and 2.4 ms in nanodiscs and native membrane, respectively, are similar (Fig. 7 a, b_3 $solid$ and $dotted$ $lines$, respectively). In native membrane, we interpreted this b-spectrum as a slightly reversible conversion of the Lumi-I/Lumi-II mixture into the Meta-Ia$_{480}$ intermediate with practically no deprotonated, 380-nm absorbing Meta-I$_{380}$ and Meta-IIa forms involved. The shape of the b-spectrum suggests that this interpretation is seemingly valid for the nanodiscs too. However, in nanodiscs at ms delay times, there is a significant amount of Meta-I$_{380}$ already present in equilibrium with Lumi-II, and thus with the earlier Lumi-I and Lumi$_{380}$ intermediates. Because the earlier equilibria are faster than this 3.1-ms transition, it is inevitable that the deprotonated forms, mostly Meta-I$_{380}$, also decay in this transition. The lack of a 380-nm peak in the b-spectrum for the nanodiscs indicates that an equivalent amount of deprotonated intermediate, the Meta-IIa in the scheme, is formed in the 3.1-ms transition. This is clearly seen in Fig. 8 a, where

the concentration time profiles of Meta-Ia and Meta-IIa are shown ($magenta$ and $orange$ $solid$ $lines$, respectively). The relative concentration of Meta-IIa present in the millisecond time range is much higher in the nanodiscs ($solid$ $lines$) than in the native membrane ($dotted$ $lines$).

The fourth b-spectrum for bovine rhodopsin in nanodiscs has a similar shape but much lower amplitude than the corresponding b-spectrum obtained for the protein in the native membrane (Fig. 7 a, b_4 $solid$ and $dotted$ $lines$, respectively). The corresponding lifetime in nanodiscs is longer (120 ms) than in native membrane (23 ms). These b-spectra represent the second step of Meta-I$_{480}$ formation, and more evidently, they show the last step of deprotonation that adjusts the balance between the protonated and deprotonated final intermediates, the Meta-Ib$_{480}$ and Meta-IIb in the scheme. In nanodiscs, this adjustment is very small compared to that in the native membrane, which indicates that in nanodiscs most of the deprotonation occurs in earlier steps, as seen in Fig. 9 and Fig. S4 c.

Despite the differences in the early kinetics of bovine rhodopsin in native membrane and nanodiscs, the final products of the reaction are similar in both environments (Fig. 8), showing practically the same ratio between the protonated and deprotonated intermediates. Thus, replacement of native lipids in the membrane around the protein with those in the nanodiscs has no significant effect on the composition of the intermediates present at the final, active state.

Human rhodopsin

The b-spectra for human rhodopsin in nanodiscs and in native membrane are compared in Fig. 7 b ($solid$ and $dotted$ $lines$, respectively). Interpretation of the first b-spectra (b_1 curves) in terms of the early kinetic steps was presented above. In addition to the Lumi-I-to-Lumi-II transition, a branching to a 380-nm absorbing intermediate, Lumi$_{380}$ was introduced. In native membrane the only significant deprotonation occurred on a much longer, the millisecond timescale. The lifetime corresponding to the first b-spectrum of human rhodopsin in native membrane was roughly twice as long as found for bovine rhodopsin and the one reported here for human rhodopsin in nanodiscs. Replacing the first lifetime for human rhodopsin in native membrane with the value found in nanodiscs (22 μs) did not affect the shape and size of the corresponding first b-spectrum significantly, and is used here for easier comparison. Despite the significant Lumi$_{380}$ formation in human nanodiscs, as seen in the first b-spectrum and in the flow through the Lumi-I-to-Lumi$_{380}$ step in Fig. 9, this intermediate does not accumulate to any significant level (Fig. 8 b, $brown$ $solid$ $line$). As already discussed for bovine rhodopsin above, the fast conversion of Lumi$_{380}$ to Meta-I$_{380}$, revealed by the amount of flow in Fig. 9 and Fig. S4 b ($blue$ $dotted$ $line$), prevents it.

The second b-spectrum for the human nanodiscs sample has a 310 μs lifetime and shows significant conversion of the Lumi-I/Lumi-II mixture into Meta-I$_{380}$ (Fig. 7 b, b_2 $solid$

curve). As in bovine rhodopsin, this transition was absent in the native membrane sample (Fig. 7 *b*, b_2 *dotted curve*). The flow through the $Lumi_{380}$-to-Meta-I_{380} step and the flow through the Lumi-II-to-Meta-I_{380} step (Fig. 9) both contribute to the buildup of Meta-I_{380} concentration (Fig. 8 *b*, *cyan curve*).

The third *b*-spectrum for the nanodisc sample has the same shape but somewhat lower amplitude than the corresponding one for the native membrane (Fig. 7 *b*, b_3 *solid and dotted curves*, respectively). Its 6.1 ms lifetime is similar to the 5.6 ms lifetime observed for the native membrane. In contrast to bovine rhodopsin, this *b*-spectrum shows a significant net deprotonation leading to the buildup of the Meta-IIa intermediate concentration. A comparison of the magenta and orange curves in Fig. 8 *b* to those in Fig. 8 *a* shows that the ratio of the deprotonated Meta-IIa to the protonated Meta-Ia is much higher for human than for bovine rhodopsin in both the native membrane (*dotted lines*) and nanodiscs (*solid lines*). The Meta-IIa intermediate of human rhodopsin is formed almost entirely from Meta-I_{380} (Fig. 9; Fig. S4 *b*, *green dotted line*), and very little from Meta-Ia_{480} (Fig. 9; Fig. S4 *c*, *red dotted line*).

As for bovine rhodopsin, the fourth *b*-spectrum for human rhodopsin in nanodiscs has significantly lower amplitude than the one in native membrane (Fig. 7 *b*, b_4 *solid and dotted curves*, respectively), and its lifetime is longer: 120 ms versus 22 ms. The final adjustment between the protonated and deprotonated forms occurs through the earliest, the Lumi-I-to-$Lumi_{380}$ and Lumi-II-to-Meta-I_{380} steps (Fig. 9; Fig. S4 *c*, *blue and green dotted lines*), and not through the deprotonation of the two Meta-I_{480} intermediates (Fig. 9; Fig. S4 *c*, *red and cyan dotted lines*).

The time-independent *b*-spectra for human rhodopsins in nanodiscs and native membrane are practically the same (Fig. 7 *b*, b_0 *solid and dotted lines*, respectively). As with bovine rhodopsin, the specificity of lipids is not crucial for the final equilibrium; it plays a role only at early times in the reaction under these experimental conditions.

The influence of protein structure and membrane lipids on the kinetics

Based on the detailed description of bovine and human rhodopsin kinetics in native membrane and nanodiscs given above, we can make two suggestions discussed in details below. The first, and perhaps the more important suggestion, is that the protein sequence and structure plays the dominant role in shaping the kinetics in membrane environments. The second suggestion is that lipids surrounding the protein modulate the kinetics by enhancing or reducing the difference induced by protein structure, or they shift the kinetic changes in time.

The structure of the protein controls the degree of deprotonation of the Schiff base. It is best viewed by comparing the composition of the end products shown in the time-inde-

pendent *b*-spectra. The fraction of the deprotonated form is higher for human than bovine rhodopsin for both native membrane and nanodiscs. Thus, the potential loss of or reduction in membrane integrity during the preparation of human rhodopsin was negligible or absent, and did not contribute to the difference between bovine and human rhodopsin seen in their native membranes. Rather, the difference is a characteristic of the protein sequence. The enhanced deprotonation of the Schiff base is seen not only in the composition of the end products but also along the reaction path at early times. Schiff base deprotonation is influenced by the distance between the Schiff base proton and its counter ion, and by factors that contribute to the stability of ion pairs, such as the presence, orientation, and mobility of water molecules and other polar groups in the vicinity of the Schiff base (46). Furthermore, a recent comparison of the bovine and human rhodopsin has suggested some possible structural differences caused by the sequence difference (26). The Thr-297, Ser-298, and Val-300 in the bovine protein, located in the vicinity of the Schiff base, are Ser-297, Ala-298, and Ile-300 in human rhodopsin. This difference could allow the human rhodopsin to accommodate an extra water molecule near the retinal pocket, as seen in Fig. 3 of (26), that can potentially affect the Schiff base deprotonation equilibrium by changing the hydrogen-bonding network (47–49). Additionally, some changes in residues 194–198 between the bovine and human rhodopsin could indicate a difference in secondary structure between the transmembrane-5 and extracellular loop-2 (26). Such a movement in this region has been suggested to be associated with Meta-I formation (26).

Although the specificity of lipids in the membrane does not seem to affect in any significant way the degree of deprotonation seen at the end of the reaction chain, it influences the timing of the deprotonation, i.e., when in the reaction sequence the deprotonation takes place. In nanodiscs the deprotonation is seen earlier than in native membranes for both rhodopsins. In native membrane, the deprotonation of the Schiff base is seen only in the *b*-spectra with millisecond lifetimes, whereas in nanodiscs, significant deprotonation occurs in the hundred-microsecond time window and much less at late-millisecond times. In nanodiscs, the experimental data are adequately fit with sets of microscopic rate constants that show almost complete control of the deprotonation process by the early steps. Both bovine and human rhodopsins follow this trend in reaching the final stage. The lipids surrounding the protein can influence the kinetics in many ways, such as through charges located on the membrane surface or restricting mobility of protein residues (28,29). The nanodiscs used in this experiment are composed predominantly of zwitterionic PC lipid molecules, which behave like neutral lipids at pH 8.7, whereas the native membrane contains a variety of neutral and charged lipids. Also, the packing of the lipids can differ in the two membrane structures because of the presence of

different unsaturated bonds in the hydrocarbon chains (29,50). Various studies have discussed the lipid-protein interactions and the sensitivity of the Meta-I-Meta-II equilibrium to lipids (28,29). Some lipid conditions that are suggested to favor the Schiff base deprotonated states (Meta-II) include addition of PE, lipids with charged amino groups or lipids with polyunsaturated acyl chains, like docosahexaenoic acid (29,50–54). Furthermore, addition of cholesterol, between 0 and 30 mol %, into PC vesicles shifts the Schiff base equilibrium toward the protonated state (Meta-I) (50).

The degree of reversibility of the Lumi-II-to-Meta-Ia$_{480}$ step, the crucial step leading to the introduction of the extended new scheme, is quite different for the bovine and human rhodopsins and it appears to be controlled almost entirely by the protein structure with little or no effect on it by the specificity of the lipids in the membrane. The degree of reversibility, the ratio of the microscopic rate constants of the backward and forward steps, is around 0.1 or less for the bovine rhodopsin, whereas it is around 0.5–0.6 for human rhodopsin. The high level of reversibility creates and maintains a very similar composition of the protonated intermediates in a wide time window and this is why the second, third, and fourth *b*-spectra of the human rhodopsin in nanodiscs have such similar shapes in Fig. 3 *b*. The difference in the degree of reversibility is also seen in Fig. 8. For human rhodopsin in both nanodiscs and native membrane, the time-dependent concentration curve for the Meta-Ia$_{480}$ intermediate (see Fig. 8 *b*, *magenta line*) overlaps considerably with the tail of the concentration curve for Lumi-II intermediate (Fig. 8 *b*, *red line*). For bovine rhodopsin there is hardly any overlap (Fig. 8 *a*). How the protein controls the reversibility of the kinetic steps, and whether it has any significance for protein activation, is unclear.

CONCLUSIONS

This study was conducted to further understand the role of protein structure and membrane environment in the photoactivation kinetics of rhodopsin, particularly the differences of the Schiff base protonation equilibrium and the reversibility of the Meta-Ia$_{480}$ formation observed previously between the bovine and human rhodopsin in their native membranes (25). For this, the activation kinetics of human and bovine rhodopsins incorporated into POPC nanodiscs was investigated at 15°C (pH 8.7) with TROA measurements. These conditions were chosen because they make it possible to observe the most photointermediates involved in rhodopsin activation and allowed us to determine detailed effects of the membrane environment on the kinetics. The photoactivation kinetics of human and bovine rhodopsin in nanodiscs under this condition is best-described using the eight-membered multisquare kinetic model, which is an extension of the previously described double-square model (5,25). The bovine and human rhodopsins in nanodiscs compared to the native membrane show the different membrane environment plays an important role in the timing of the Schiff base deprotonation. This is identified through an early Schiff base deprotonation, observed as the Lumi$_{380}$ intermediate, concurrent with the Lumi-I/Lumi-II step. However, the type of lipid in the membrane does not appear to be crucial for the final Schiff base protonation equilibrium and the reversibility of Meta-Ia$_{480}$ formation under these conditions. The fraction of Schiff base deprotonation is higher in human rhodopsin in comparison to the bovine rhodopsin in both native membrane and nanodiscs. This suggests that the protein sequence and structure plays the dominant role in the difference observed between the human and bovine rhodopsin.

The kinetic steps depicted in the eight-membered multisquare model, and clearly observed under our experimental conditions, may become obscured under more physiological conditions. Even when specific combinations of the microscopic rates prevent the detection of some of the intermediates and steps in the complex scheme, the intermediates are still essential parts of the protein dynamics. Additionally, as many studies are conducted under different lipid environments (detergent, nanodiscs, liposomes, etc.) (28,51,55,56), temperatures, and pHs, it is important to understand the effect of these conditions on the intricate activation mechanism of rhodopsin.

SUPPORTING MATERIAL

AUTHOR CONTRIBUTIONS

I.S. carried out all of the kinetic data analysis. C.F. prepared the rhodopsin samples and carried out optical spectroscopic experiments. Y.G. prepared all nanodisc samples. E.C.Y.Y. supervised the nanodisc sample preparation. D.S.K. developed the original idea for the experiment and supervised the optical experiments. All authors were involved in drafting the text.

ACKNOWLEDGMENTS

SUPPORTING CITATIONS

Reference (57) appears in the Supporting Material.

REFERENCES

1. Wald, G. 1968. Molecular basis of visual excitation. *Science.* 162: 230–239.

2. Matthews, R. G., R. Hubbard, ..., G. Wald. 1963. Tautomeric forms of Metarhodopsin. *J. Gen. Physiol.* 47:215–240.

3. Yoshizawa, T. 1972. The behaviour of visual pigments at low temperatures. *In* Handbook of Sensory Physiology. Springer, Berlin-Heidelberg, New York, pp. 145–179.

4. Jäger, S., I. Szundi, ..., D. S. Kliger. 1998. Effects of pH on rhodopsin photointermediates from lumirhodopsin to metarhodopsin II. *Biochemistry.* 37:6998–7005.

5. Szundi, I., C. Funatogawa, and D. S. Kliger. 2016. Complexity of bovine rhodopsin activation revealed at low temperature and alkaline pH. *Biochemistry.* 55:5095–5105.

6. Szundi, I., J. W. Lewis, and D. S. Kliger. 2003. Two intermediates appear on the lumirhodopsin time scale after rhodopsin photoexcitation. *Biochemistry.* 42:5091–5098.

7. Thorgeirsson, T. E., J. W. Lewis, ..., D. S. Kliger. 1992. Photolysis of rhodopsin results in deprotonation of its retinal Schiff's base prior to formation of metarhodopsin II. *Photochem. Photobiol.* 56:1135–1144.

8. Thorgeirsson, T. E., J. W. Lewis, ..., D. S. Kliger. 1993. Effects of temperature on rhodopsin photointermediates from lumirhodopsin to metarhodopsin II. *Biochemistry.* 32:13861–13872.

9. Monger, T. G., R. R. Alfano, and R. H. Callender. 1979. Photochemistry of rhodopsin and isorhodopsin investigated on a picosecond time scale. *Biophys. J.* 27:105–115.

10. Peters, K., M. L. Applebury, and P. M. Rentzepis. 1977. Primary photochemical event in vision: proton translocation. *Proc. Natl. Acad. Sci. USA.* 74:3119–3123.

11. Schoenlein, R. W., L. A. Peteanu, ..., C. V. Shank. 1991. The first step in vision: femtosecond isomerization of rhodopsin. *Science.* 254:412–415.

12. Hug, S. J., J. W. Lewis, ..., D. S. Kliger. 1990. Nanosecond photolysis of rhodopsin: evidence for a new, blue-shifted intermediate. *Biochemistry.* 29:1475–1485.

13. Lewis, J. W...., 1990. Direct evidence for an equilibrium between early photolysis intermediates of rhodopsin. *J. Am. Chem. Soc.* 112:6711–6712.

14. Choe, H. W., Y. J. Kim, ..., O. P. Ernst. 2011. Crystal structure of metarhodopsin II. *Nature.* 471:651–655.

15. Kimata, N., A. Pope, ..., S. O. Smith. 2016. Free backbone carbonyls mediate rhodopsin activation. *Nat. Struct. Mol. Biol.* 23:738–743.

16. Kimata, N., P. J. Reeves, and S. O. Smith. 2015. Uncovering the triggers for GPCR activation using solid-state NMR spectroscopy. *J. Magn. Reson.* 253:111–118.

17. Patel, A. B., E. Crocker, ..., S. O. Smith. 2005. Changes in interhelical hydrogen bonding upon rhodopsin activation. *J. Mol. Biol.* 347:803–812.

18. Pope, A., M. Eilers, ..., S. O. Smith. 2014. Amino acid conservation and interactions in rhodopsin: probing receptor activation by NMR spectroscopy. *Biochim. Biophys. Acta.* 1837:683–693.

19. Salgado, G. F., A. V. Struts, ..., M. F. Brown. 2006. Solid-state 2H NMR structure of retinal in metarhodopsin I. *J. Am. Chem. Soc.* 128:11067–11071.

20. Ye, S., E. Zaitseva, ..., R. Vogel. 2010. Tracking G-protein-coupled receptor activation using genetically encoded infrared probes. *Nature.* 464:1386–1389.

21. Altenbach, C., A. K. Kusnetzow, ..., W. L. Hubbell. 2008. High-resolution distance mapping in rhodopsin reveals the pattern of helix movement due to activation. *Proc. Natl. Acad. Sci. USA.* 105:7439–7444.

22. Knierim, B., K. P. Hofmann, ..., W. L. Hubbell. 2007. Sequence of late molecular events in the activation of rhodopsin. *Proc. Natl. Acad. Sci. USA.* 104:20290–20295.

23. Nathans, J., and D. S. Hogness. 1984. Isolation and nucleotide sequence of the gene encoding human rhodopsin. *Proc. Natl. Acad. Sci. USA.* 81:4851–4855.

24. Wald, G., and P. K. Brown. 1958. Human rhodopsin. *Science.* 127:222–226.

25. Funatogawa, C., I. Szundi, and D. S. Kliger. 2016. A Comparison between the photoactivation kinetics of human and bovine rhodopsins. *Biochemistry.* 55:7005–7013.

26. Kazmin, R., A. Rose, ..., F. J. Bartl. 2015. The activation pathway of human rhodopsin in comparison to bovine rhodopsin. *J. Biol. Chem.* 290:20117–20127.

27. Boesze-Battaglia, K., and A. D. Albert. 1992. Phospholipid distribution among bovine rod outer segment plasma membrane and disk membranes. *Exp. Eye Res.* 54:821–823.

28. Jastrzebska, B., A. Debinski, ..., K. Palczewski. 2011. Role of membrane integrity on G protein-coupled receptors: rhodopsin stability and function. *Prog. Lipid Res.* 50:267–277.

29. Soubias, O., and K. Gawrisch. 2012. The role of the lipid matrix for structure and function of the GPCR rhodopsin. *Biochim. Biophys. Acta.* 1818:234–240.

30. Fliesler, S. J., and R. E. Anderson. 1983. Chemistry and metabolism of lipids in the vertebrate retina. *Prog. Lipid Res.* 22:79–131.

31. Martinez, M., A. Ballabriga, and J. J. Gil-Gibernau. 1988. Lipids of the developing human retina: I. Total fatty acids, plasmalogens, and fatty acid composition of ethanolamine and choline phosphoglycerides. *J. Neurosci. Res.* 20:484–490.

32. Denisov, I. G., and S. G. Sligar. 2016. Nanodiscs for structural and functional studies of membrane proteins. *Nat. Struct. Mol. Biol.* 23:481–486.

33. Chung, K. Y., P. W. Day, ..., B. K. Kobilka. 2013. Identification of GPCR-interacting cytosolic proteins using HDL particles and mass spectrometry-based proteomic approach. *PLoS One.* 8:e54942.

34. Banerjee, S., T. Huber, and T. P. Sakmar. 2008. Rapid incorporation of functional rhodopsin into nanoscale apolipoprotein bound bilayer (NABB) particles. *J. Mol. Biol.* 377:1067–1081.

35. Liu, M. Y., J. Liu, ..., E. C. Yan. 2013. Thermal stability of rhodopsin and progression of retinitis pigmentosa: comparison of S186W and D190N rhodopsin mutants. *J. Biol. Chem.* 288:17698–17712.

36. Rakoczy, E. P., C. Kiel, ..., L. Serrano. 2011. Analysis of disease-linked rhodopsin mutations based on structure, function, and protein stability calculations. *J. Mol. Biol.* 405:584–606.

37. Lewis, J. W., F. J. van Kuijk, ..., D. S. Kliger. 1991. Photolysis intermediates of human rhodopsin. *Biochemistry.* 30:11372–11376.

38. van Kuijk, F. J., J. W. Lewis, ..., D. S. Kliger. 1991. Spectrophotometric quantitation of rhodopsin in the human retina. *Invest. Ophthalmol. Vis. Sci.* 32:1962–1967.

39. Denisov, I. G., Y. V. Grinkova, ..., S. G. Sligar. 2004. Directed self-assembly of monodisperse phospholipid bilayer Nanodiscs with controlled size. *J. Am. Chem. Soc.* 126:3477–3487.

40. Bayburt, T. H., Y. V. Grinkova, and S. G. Sligar. 2002. Self-assembly of discoidal phospholipid bilayer nanoparticles with membrane scaffold proteins. *Nano Lett.* 2:853–856.

41. Denisov, I. G., B. J. Baas, ..., S. G. Sligar. 2007. Cooperativity in cytochrome P450 3A4: linkages in substrate binding, spin state, uncoupling, and product formation. *J. Biol. Chem.* 282:7066–7076.

42. Boldog, T., M. Li, and G. L. Hazelbauer. 2007. Using Nanodiscs to create water-soluble transmembrane chemoreceptors inserted in lipid bilayers. *Methods Enzymol.* 423:317–335.

43. Mitra, N., Y. Liu, ..., E. C. Yan. 2013. Calcium-dependent ligand binding and G-protein signaling of family B GPCR parathyroid hormone 1 receptor purified in nanodiscs. *ACS Chem. Biol.* 8:617–625.

44. Lewis, J. W., and D. S. Kliger. 1991. Rotational diffusion effects on absorbance measurements: limitations to the magic-angle approach. *Photochem. Photobiol.* 54:963–968.

45. Szundi, I., J. W. Lewis, and D. S. Kliger. 1997. Deriving reaction mechanisms from kinetic spectroscopy. Application to late rhodopsin intermediates. *Biophys. J.* 73:688–702.

46. Yan, E. C.…, 2007. Photointermediates of the rhodopsin S186A mutant as a probe of the hydrogen-bond network in the chromophore pocket and the mechanism of counterion switch. *J. Phys. Chem. C.* 111:8843–8848.

47. Vogel, R., F. Siebert, …, M. Sheves. 2006. Modulating rhodopsin receptor activation by altering the pKa of the retinal Schiff base. *J. Am. Chem. Soc.* 128:10503–10512.

48. Yan, E. C., M. A. Kazmi, …, T. P. Sakmar. 2002. Function of extracellular loop 2 in rhodopsin: glutamic acid 181 modulates stability and absorption wavelength of metarhodopsin II. *Biochemistry.* 41:3620–3627.

49. Yan, E. C., M. A. Kazmi, …, R. A. Mathies. 2003. Retinal counterion switch in the photoactivation of the G protein-coupled receptor rhodopsin. *Proc. Natl. Acad. Sci. USA.* 100:9262–9267.

50. Mitchell, D. C., M. Straume, …, B. J. Litman. 1990. Modulation of metarhodopsin formation by cholesterol-induced ordering of bilayer lipids. *Biochemistry.* 29:9143–9149.

51. Brown, M. F. 1994. Modulation of rhodopsin function by properties of the membrane bilayer. *Chem. Phys. Lipids.* 73:159–180.

52. Gibson, N. J., and M. F. Brown. 1993. Lipid headgroup and acyl chain composition modulate the MI-MII equilibrium of rhodopsin in recombinant membranes. *Biochemistry.* 32:2438–2454.

53. Soubias, O., W. E. Teague, Jr., …, K. Gawrisch. 2010. Contribution of membrane elastic energy to rhodopsin function. *Biophys. J.* 99:817–824.

54. Gibson, N. J., and M. F. Brown. 1991. Role of phosphatidylserine in the MI-MII equilibrium of rhodopsin. *Biochem. Biophys. Res. Commun.* 176:915–921.

55. Serebryany, E., G. A. Zhu, and E. C. Yan. 2012. Artificial membrane-like environments for in vitro studies of purified G-protein coupled receptors. *Biochim. Biophys. Acta.* 1818:225–233.

56. Soubias, O., and K. Gawrisch. 2013. Rhodopsin-lipid interactions studied by NMR. *Methods Enzymol.* 522:209–227.

57. Cai, Y., Y. Liu, …, E. C. Y. Yan. 2017. Purification of family B G protein-coupled receptors using nanodiscs: application to human glucagon-like peptide-1 receptor. *PLoS One.* 12:e0179568.